Virology 399 (2010) 257–269

Contents lists available at ScienceDirect

Virology

journal homepage: www.elsevier.com/locate/yviro

Identification of *N*-linked carbohydrates from severe acute respiratory syndrome (SARS) spike glycoprotein

Gayle Ritchie [a], David J. Harvey [a,*], Friederike Feldmann [b,c], Ute Stroeher [b,d], Heinz Feldmann [b,c,d], Louise Royle [e], Raymond A. Dwek [a], Pauline M. Rudd [f]

[a] Oxford Glycobiology Institute, Department of Biochemistry, South Parks Road, Oxford OX1 3QU, UK
[b] Special Pathogens Program, National Microbiology Laboratory, Public Health Agency of Canada, Winnipeg, Manitoba, Canada
[c] Rocky Mountain Laboratories, Division of Intramural Research, National Institute of Allergy and Infectious Diseases, National Institutes of Health, Hamilton, Montana, USA
[d] Department of Medical Microbiology, University of Manitoba, Winnipeg, Manitoba, Canada
[e] Ludger Ltd, Culham Science Centre, Abingdon, Oxfordshire, OX14 3EB, UK
[f] National Institute for Bioprocessing Research and Training, Conway Institute, University College Dublin, Belfield, Dublin 4, Ireland

ARTICLE INFO

Article history:
Received 30 June 2009
Returned to author for revision
2 November 2009
Accepted 16 December 2009
Available online 2 February 2010

Keywords:
SARS
Spike glycoprotein
Glycosylation
N-Linked
Mass Spectrometry
Negative ion fragmentation

ABSTRACT

N-glycans were released from the SARS coronavirus (SARS-CoV) spike glycoprotein produced in Vero E6 cells and their structures were determined by a combination of matrix-assisted laser desorption/ionization (MALDI) mass spectrometry, negative ion electrospray collision-induced dissociation time-of-flight mass spectrometry and normal-phase high-performance liquid chromatography with exoglycosidase digestion. Major glycans were high-mannose ($Man_{5-9}GlcNAc_2$), hybrid and bi-, tri- and tetra-antennary complex with and without bisecting GlcNAc and core fucose. Complex glycans with fewer than the full complement of galactose residues were present and sialylation was negligible. Treatment with the glucosidase inhibitor *N*-butyl-deoxynojirimycin (*N*B-DNJ) inhibited *N*-glycan processing as evidenced by the appearance of glycans of composition $Glc_3Man_{7-9}GlcNAc_2$. However, some complex glycans remained suggesting the presence of an α-endomannosidase. Our data in tissue culture indicate that inhibition of *N*-glycan processing may be considered as a therapeutic strategy against SARS CoV infections.

Introduction

The aetiological agent of the severe acute respiratory syndrome (SARS) is a coronavirus (SARS-CoV) which was responsible for causing a worldwide pandemic of lower respiratory tract infection between November 2002 and July 2003 (Drosten et al., 2003; Ksiazek et al., 2003; Marra et al., 2003; Rota et al., 2003). During this time, there were approximately 8100 probable SARS cases and approximately 800 recorded fatalities (http://www.wpro.who.int/sars/). Rapid identification of individuals presenting with the disease as well as appropriate nursing techniques and quarantine procedures allowed the outbreak to be controlled by July of 2003. There have since been smaller outbreaks of the disease, but these have been contained with minimal secondary transmission. In the clinic, SARS-CoV infection presents as atypical pneumonia, with patients reporting symptoms of high fever (>38 °C), dry cough, shortness of breath (dyspnea) and/or more severe breathing difficulties, which may occasionally require mechanical ventilation. The viral reservoirs are presumed to be bats (Wang and Eaton, 2007; Wang et al., 2006) and the palm civet cat has been implicated as a carrier of the virus, though there may also be other asymptomatic animal carriers (Shi and Hu, 2008).

Of the several proteins found in the SARS coronavirus (Tan et al., 2006; Ying et al., 2004), the large SARS-CoV spike glycoprotein (S) (Tripet et al., 2004) located on the virion surface is involved in both target cell attachment and fusion processes (Yang et al., 2004). As with several coronaviruses, the spike glycoprotein can be proteolytically cleaved into two non-covalently associated glycoproteins: the virion-associated S1 (666 amino acid residues) containing the receptor attachment site and the transmembrane-anchored S2 (583 residues) responsible for fusion activity (Bergeron et al., 2005; Follis et al., 2006; Li et al., 2005).

The SARS-CoV S glycoprotein is a 1255-amino acid precursor polypeptide as deduced from the published genome sequence and has

Abbreviations: 2AB, 2-Aminobenzamide; ACE2, angiotensin converting enzyme 2; CoV, coronavirus; CPE, cytopathic effects; DHB, 2,5-dihydroxybenzoic acid; FBS, fetal bovine serum; GU, glucose unit; HPLC, high-performance liquid chromatography; HRP, horseradish peroxidase; IgG, immunoglobulin; MALDI, matrix-assisted laser desorption/ionization; MOI, multiplicity of infection; MS, mass spectrometry; *N*B-DNJ, *N*-butyl-deoxynojirimycin; NP, normal phase; PAGE, polyacrylamide gel electrophoresis; PBS, phosphate-buffered saline; PNGase F, peptide *N*-glycosidase F; PTFE, polytetrafluoroethylene; PVDF, polyvinylidene fluoride; Q, -quadrupole; S, spike protein; SARS, severe acute respiratory syndrome; SDS, sodium dodecyl sulphate; TOF, time-of-flight.

* Corresponding author. Fax: +44 1865 275216.
E-mail address: david.harvey@bioch.ox.ac.uk (D.J. Harvey).

0042-6822/$ – see front matter © 2009 Elsevier Inc. All rights reserved.
doi:10.1016/j.virol.2009.12.020

23 potential *N*-linked glycosylation sites (Eickmann et al., 2003; Marra et al., 2003; Rota et al., 2003; Xiao et al., 2003). Previous studies have demonstrated that several of these sites are occupied and possess both complex-type and high-mannose type *N*-glycans (Krokhin et al., 2003; Song et al., 2004; Ying et al., 2004). However, full glycan analysis has not yet been performed.

SARS-CoV uses the angiotensin converting enzyme 2 (ACE2) as the primary receptor (Chen and Subbarao, 2007; Li et al., 2003; Moore et al., 2004; Wang et al., 2004) suggesting that oligomannose-containing *N*-glycans on the SARS-CoV S glycoprotein surface may be involved in mediating virus attachment to cells expressing this cell surface lectin. The C-type lectins DC-SIGN and L-SIGN (DC/L-SIGN) can enhance viral entry (Marzi et al., 2004; Yang et al., 2004). Site-directed mutagenesis analyses have identified seven glycosylation sites on the S protein critical for DC/L-SIGN-mediated virus entry. They include asparagine residues 109, 118, 119, 158, 227, 589, and 699, which are distinct from residues of the ACE2-binding domain (amino acids 318–510) (Han et al., 2007). Recently, L-SIGN (DC-SIGNR) has been shown to act as an entry receptor for SARS-CoV infection (Jeffers et al., 2004), and its expression in lung alveolar and liver cells correlates with the disease pathogenesis observed in these organs in many SARS patients.

Given that oligomannose *N*-glycans may be involved in viral attachment to cells it is of interest to study the effects of modifications to the *N*-glycan profile with the object of possibly identifying therapeutic strategies. This report describes the first complete *N*-glycosylation analysis of SARS-CoV S glycoprotein produced in Vero E6 cells, a cell line derived from African green monkeys, and demonstrates the inhibitory effect of the α-glucosidase inhibitor *N*-butyl-deoxynojirimycin (*N*B-DNJ) on virus replication in this cell line.

Results and discussion

Characterization of SARS-CoV spike protein

Viral proteins from purified viral particles were separated on 9% SDS-PAGE gels and stained with Coomassie blue (Fig. 1). The proteins S, M and N were detected but the gel was not dense enough to detect the smaller (7 kDa) E protein. Western blotting using the SARS-CoV S glycoprotein antibody (Imgenex) confirmed the identity and molecular weight (180 kDa) of the S protein which was consistent with earlier reports (Krokhin et al., 2003; Song et al., 2004; Xiao et al., 2003) and indicated the presence of the fully modified glycoprotein. There was no apparent difference in molecular weight between the glycoproteins produced with and without *N*B-DNJ.

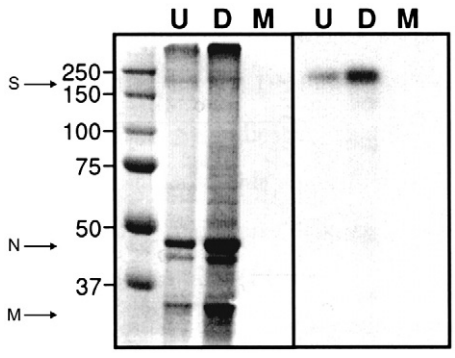

Fig. 1. SDS-PAGE and western blotting analysis of purified SARS-CoV (strain Tor2) preparation. Left panel: 9% SDS-PAGE analysis of SARS-CoV virion preparation. S = SARS-CoV spike glycoprotein, N = SARS-CoV nucleoprotein, M = SARS-CoV matrix protein. Molecular weight markers are shown on the left. Right panel: Western blotting analysis of SARS-Co V virion preparation using an anti-SARS-CoV S antibody (Imgenex). U, untreated preparation; D, drug(*N*B-DNJ) treated preparation; M, mock infected preparation.

Identification of N-glycans

The spike glycoprotein-containing band was cut from the gel for *N*-glycan analysis by in-gel PNGase F digestion followed by HPLC (as 2AB derivatives), exoglycosidase digestion, MALDI-TOF and nanoelectrospray MS/MS as described below. The HPLC trace of the SARS-CoV glycans obtained without *N*B-DNJ treatment is shown in Fig. 2a. Traces obtained before and after digestion with *Arthrobacter ureafaciens* sialidase (Fig. 2b) were virtually identical showing negligible incorporation of sialic acid in these glycans. Previous work (Feldmann et al., 1994) has also shown a lack of sialylated *N*-glycans in Marburg virus grown in Vero E6 cells. The positive ion MALDI (Fig. 3) and negative ion nanoelectrospray spectra were similar to each other and to the HPLC trace although more glycans were resolved by mass spectrometry. Table 1 lists the identified glycans and their percentage of the total glycan pool as measured by MALDI-TOF MS and Table 2 lists the percentage of various compound glycan types. Because a few of the glycans with different structures had the same mass and were, thus, not separated by mass spectrometry, the figures should be taken as approximate. Nevertheless, they reflect the composition of the mixture reasonably accurately.

The glycans were identified by exoglycosidase digestion with monitoring by HPLC and by negative ion MS/MS of their $[M+H_2PO_4]^-$ ions (Harvey, 2005a) using electrospray sample introduction (Harvey, 2005b,c; Harvey et al., 2008b). The HPLC traces obtained after ABS and bovine testis β-galactosidase (BTG) treatment (Fig. 2c) confirmed attachment of galactose at the non-reducing termini of the glycan antenna. Further incubation with hexosaminidase (Fig. 2d) reduced the profile to $Man_3GlcNAc_2$, $Man_3GlcNAc_2Fuc_1$ and a series of unaffected high-mannose glycans. A few compounds were present at concentrations that were too weak to permit acquisition of informative MS/MS spectra. However, their structures could be deduced from the structures of related compounds, e.g., complex glycans with different numbers of galactose residues. Such compounds are identified in Table 1. Ion nomenclature in the following discussion follows that introduced by Domon and Costello (1988) as modified by Harvey et al. (2004) by the use of the subscript "R" to specify cleavages adjacent to the reducing-terminal GlcNAc residue

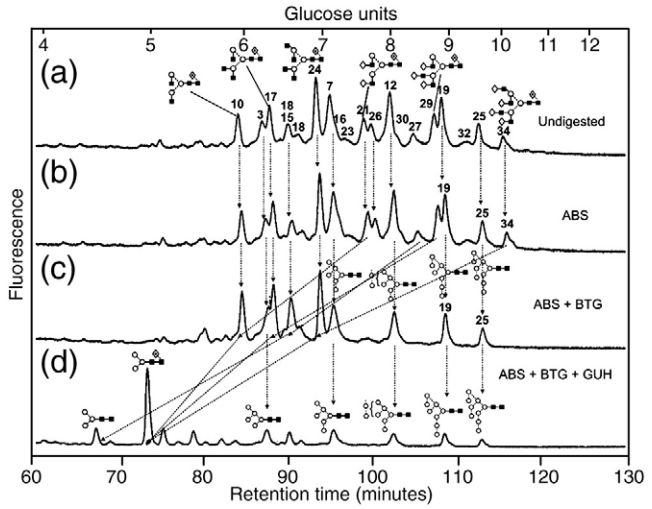

Fig. 2. (a) NP-HPLC analysis of SARS-CoV S *N*-glycans. (b) HPLC analysis of SARS-CoV *N*-glycans following digestion with *Arthrobacter ureafaciens* sialidase (ABS, EC 3.2.1.18), (c) HPLC analysis following digestion with a mixture of ABS and bovine testis β-galactosidase (BTG, EC 3.2.1.23) and (d) HPLC analysis following incubation with a mixture of ABS, BTG and *Streptococcus pneumoniae* hexosaminidase (GUH, EC 3.2.1.30). The broken lines connecting the peaks in the various traces show movement of the peaks following digestion. Symbols used for the structural formulae: ■ = GlcNAc, ○ = mannose, ◊ = galactose, ◈ = fucose. The angle of the lines connecting the symbols shows the linkage with full and broken lines specifying β- and α-linkages, respectively. Further details are given in the paper by Harvey et al. (2009).

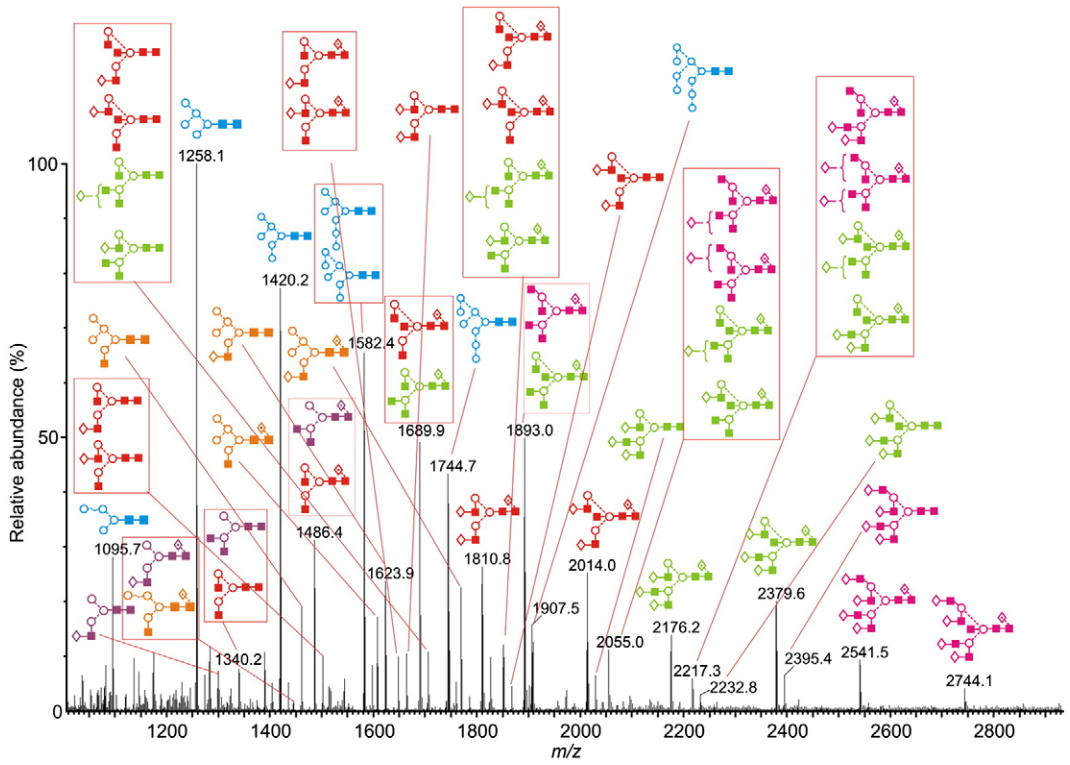

Fig. 3. Positive ion MALDI-TOF mass spectrum ($[M+Na]^+$ ions) of the *N*-linked glycans obtained from the SARS-CoV spike protein. Peaks are identified in Table 1 and the key to the structural symbols is in the legend to Fig. 2 with the addition of □ = glucose. Glycan types are coloured: blue = high mannose, orange = hybrid, purple = monoantennary, red = biantennary, green = triantennary, pink = tetra-antennary.

and "R-1" to specify cleavages adjacent to the penultimate GlcNAc in order to avoid confusion by the subscript number changing as a function of antenna length.

High-mannose glycans

High-mannose glycans containing from four to nine mannose residues were present in the glycan mixture (Fig. 3). Incubation with *Aspergillus saitoi α*-mannosidase (data not shown) reduced the larger compounds to $Man_5GlcNAc_2$ (compound **3**, Table 1) confirming the α-mannose linkages. The negative ion MS/MS spectra of the high-mannose glycans $Man_{5-9}GlcNAc_2$ (phosphate adducts) are shown in Fig. 4. The cross-ring $^{2,4}A_R$ and $^{2,4}A_{R-1}$ fragments together with the B_{R-1} ion at the high-mass end of the spectra define the 1→4-linked chitobiose core (Harvey, 2005b; Harvey et al., 2008b) and the single C_1 fragment at *m/z* 179 confirmed hexose (mannose) as the only non-reducing end residue. The ions towards the centre of the spectrum were mainly derived from the 6-antenna and allowed the distribution of the mannose residues between the two antennae to be determined. Predominant among these ions were the D-ion (formal loss of the 3-antenna from the C_{R-1} ion), the $[D-18]^-$ ion and the $^{0,3}A_{R-2}$ cross-ring cleavage fragment (core mannose residue) (Harvey, 2005b). Thus, $Man_5GlcNAc_2$ (**3**) produced a spectrum with these ions at *m/z* 647, 629 and 575, respectively. Further confirmation of the substitution pattern was provided by the C_2 ion at *m/z* 503 (three mannose residues). In the spectrum of $Man_6GlcNAc_2$ (**7**, Fig. 4b) the D, $[D-18]^-$ and $^{0,3}A_{R-2}$ ions were in the same position as in the spectrum of $Man_5GlcNAc_2$ showing that the sixth mannose was attached to the 3-antenna. These three diagnostic ions all shifted by 162 mass units to higher mass in the spectrum of $Man_7GlcNAc_2$ (**12**, Fig. 4c) showing that the seventh mannose was attached to the 6-antenna and the high abundance of the ion at *m/z* 485 was consistent with its location on the 6-branch of this antenna. This ion, termed D′, is thought to be equivalent to ion D as the result of the same substitution pattern of the branched mannose of the 6-antenna to that at the mannose of the core. This same pattern of D, $[D-18]^-$, $^{0,3}A_{R-2}$ and D′ ions was present in the spectrum of $Man_8GlcNAc_2$ (**19**, Fig. 4d) confirming attachment of the 8th mannose to the 3-antenna and indicating that this compound had the classical d1,d3-substitution pattern. Finally, in the spectrum of $Man_9GlcNAc_2$ (**25**, Fig. 4e), the three 6-antenna-derived diagnostic ions shifted upwards by another 162 mass units to *m/z* 971, 953 and 899 as the result of the extra mannose residue in the 6-antenna. The presence of a second set of the D, $[D-18]^-$, $^{0,3}A_{R-2}$ ions at *m/z* 647, 629 and 575 in the spectrum of $Man_7GlcNAc_2$ (**12**) indicated the presence of a second isomer with three mannose residues in the 3-antenna. A fragmentation spectrum was not obtained for $Man_4GlcNAc_2$ (**1**).

Hybrid glycans

Hybrid glycans (numbers **9**, **13**, **14** and **20**, Table 1) were detected in the mass spectra but were not apparent in the HPLC trace of the total glycans. However, they became visible by HPLC following incubation with Jack bean α-mannosidase which removed all of the mannose residues from the 6-antenna to leave the chitobiose core and 3-antenna which consisted of GlcNAc and Gal-GlcNAc (data not shown). Fig. 5 shows the negative ion MS/MS spectra of the hybrid glycans **9** (Fig. 5a) and **14** (Fig. 5b). The pattern of mannose substitution on the 6-antenna was determined by the masses of the D, $[D-18]^-$, $^{0,3}A_{R-2}$, D′ and $[D'-18]^-$ ions in the negative ion MS/MS spectra as described above. The spectrum of the glycan corresponding to $Hex_5GlcNAc_3$ (**9**, Fig. 5a) showed the presence of two compounds as evidenced by the appearance of two sets of D and $[D-18]^-$ ions (*m/z* 647/629 and 485/467) indicating three and two mannose residues respectively in the 6-antenna. The linkage of the mannose residue in the compounds with two mannose residues in the 6-antenna was not determined. Location of the fucose at position 6 of the terminal GlcNAc residue, when present, was determined by the masses of the

Table 1
N-linked glycans with the masse of their $[M+Na]^+$ and $[M+H_2PO_4]^-$ ions.

No.[a]	GU[b]	*m/z*				Composition			Structure[e]
		MALDI ($[M+Na]^+$)[c]		Electrospray ($[M+H_2PO_4]^-$)[d]		Hex	HexNAc	dHex	
		Found	Calc.	Found	Calc.				
1	–	1095.7	1096.0	–	1169.3	4	2	0	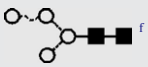
2	–	1136.9	1137.0	–	1210.4	3	3	0	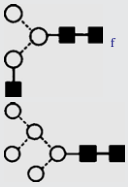
3	6.17	1258.1	1258.1	1331.4	1331.4	5	2	0	
4	–	1283.8	1283.2	1356.6	1356.4	3	3	1	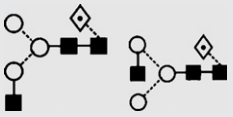
5	–	1299.4	1299.2	–	1372.4	4	3	0	
6	–	1339.9	1340.2	1413.5	1413.5	3	4	0	
7	7.05	1420.2	1420.2	1493.5	1493.5	6	2	0	
8	6.40	1444.7	1445.3	1518.5	1518.5	4	3	1	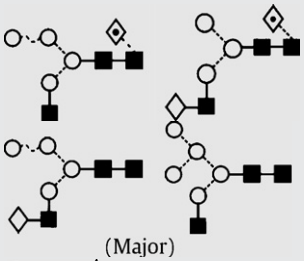
9	–	1461.4	1461.3	1534.5	1534.5	5	3	0	(Major)
10	5.89	1486.4	1486.4	1559.5	1559.5	3	4	1	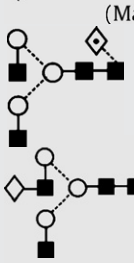
11	–	1502.0	1502.4	1575.5	1575.5	4	4	0	
12	7.94	1582.4	1582.4	1655.5	1655.5	7	2	0	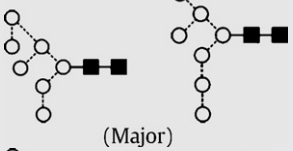 (Major)
13	–	1607.7	1607.4	1680.5	1680.5	5	3	1	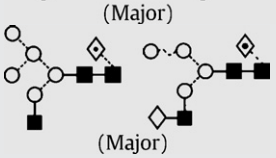 (Major)
14	–	1623.9	1623.4	1696.5	1696.5	6	3	0	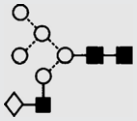

Table 1 (*continued*)

No.[a]	GU[b]	*m/z*				Composition			Structure[e]
		MALDI ($[M+Na]^+$)[c]		Electrospray ($[M+H_2PO_4]^-$)[d]		Hex	HexNAc	dHex	
		Found	Calc.	Found	Calc.				
15	6.63 6.81	1648.3	1648.5	1721.6	1721.6	4	4	1	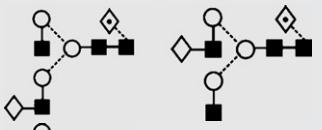
16	7.13	1664.4	1664.5	1737.6	1737.6	5	4	0	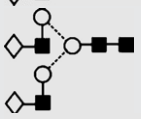
17	6.17 6.27	1689.9	1689.6	1762.6	1762.6	3	5	1	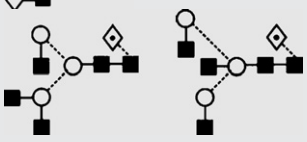
18	6.50	1705.3	1705.5	1778.5	1778.6	4	5	0	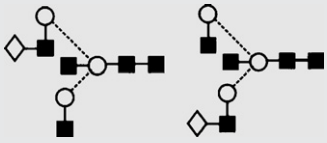
19	8.80	1744.7	1744.5	1817.6	1817.6	8	2	0	
20	—	1769.9	1769.6	1842.6	1842.6	6	3	1	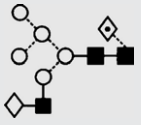
21	7.54	1810.8	1810.6	1883.6	1883.6	5	4	1	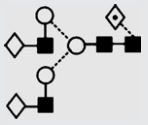
22	—	1851.9	1851.7	1924.6	1924.6	4	5	1	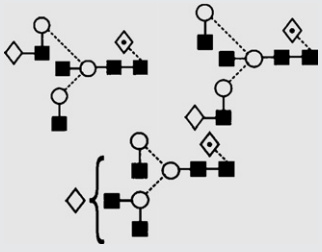
23	7.24	1867.7	1867.7	1940.6	1940.6	5	5	0	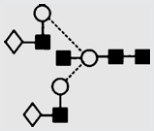
24	6.86	1893.0	1892.7	1965.6	1965.7	3	6	1	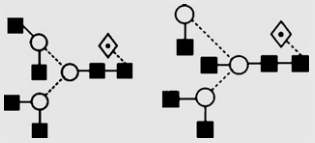
25	9.48	1907.5	1906.7	1979.6	1979.6	9	2	0	

(*continued on next page*)

Table 1 (*continued*)

No.[a]	GU[b]	*m/z*				Composition			Structure[e]
		MALDI ($[M+Na]^+$)[c]		Electrospray ($[M+H_2PO_4]^-$)[d]		Hex	HexNAc	dHex	
		Found	Calc.	Found	Calc.				
26	7.65	2014.0	2013.8	2086.7	2086.7	5	5	1	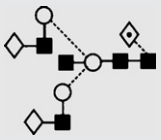
27	8.32	2029.8	2029.8	2102.7	2102.7	6	5	0	
28	8.02	2055.0	2054.9	2127.7	2127.7	4	6	1	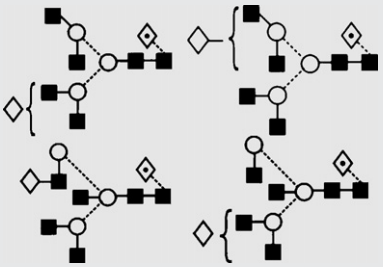
29	8.67	2176.2	2176.0	2248.7	2248.8	6	5	1	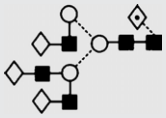
30	—	2217.3	2217.0	2289.7	2289.8	5	6	1	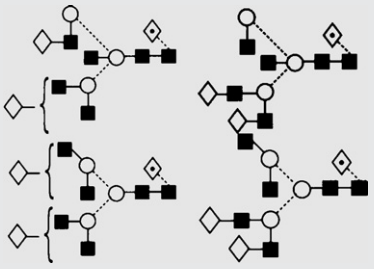
31	—	2232.8	2233.0	—	2305.8	6	6	0	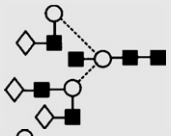
32	9.26	2379.6	2379.2	2451.8	2451.8	6	6	1	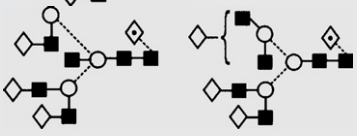
33	—	2395.4	2395.2	—	2467.8	7	6	0	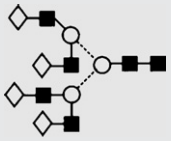
34	9.95	2541.5	2541.3	2613.8	2613.9	7	6	1	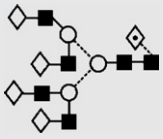
35	—	2744.1	2744.5	—	2817.0	7	7	1	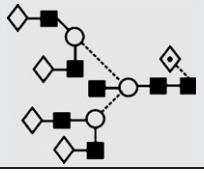 [f]

Table 1 (*continued*)

No.[a]	GU[b]	*m/z*				Composition			Structure[e]
		MALDI ($[M+Na]^+$)[c]		Electrospray ($[M+H_2PO_4]^-$)[d]		Hex	HexNAc	dHex	
		Found	Calc.	Found	Calc.				
36[g]	10.27	–	–	–	–	10	2	0	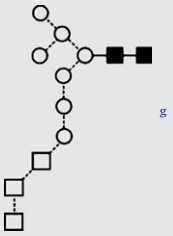 [g]
37[g]	11.16	–	–	–	–	11	2	0	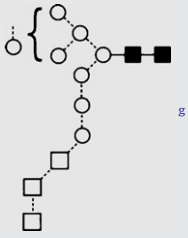 [g]
38[g]	11.80	–	–	–	–	12	2	0	 [g]

[a] Peak numbers as in the MALDI-TOF spectrum (Fig. 3).
[b] Glucose unit.
[c] Average mass.
[d] Monoisotopic mass.
[e] Symbols used for the structural formulae: ■ = GlcNAc, ○ = mannose, ◊ = galactose, ◈ = fucose, □ = glucose. The angle of the lines connecting the symbols shows the linkage with full and broken lines specifying β- and α-linkages, respectively.
[g] In the presence of *N*B-DNJ only.
[f] Not confirmed by fragmentation.

abundant $^{2,4}A_R$, $^{2,4}A_{R-1}$ and B_{R-1} ions in the MS/MS spectra (Harvey, 2005c; Harvey et al., 2008b) all of which were formed by loss of the fucose residue as the result of its attachment to the eliminated neutral fragment. Structures are shown in Table 1. No antenna-substituted fucose was detected in these or in the spectra of the complex glycans. The composition of the 3-antenna was specified by the mass of an E-type cross-ring fragment ion (substituents plus 101 mass units from the mannose residue (Harvey, 2005c; Harvey et al., 2008b)). These ions were of low abundance but were present at *m/z* 304 and 466 in the spectrum shown in Fig. 5a and at *m/z* 466 in Fig. 5b confirming the presence of GlcNAc and Gal-GlcNAc antennae respectively. The 3-antenna composition was further defined by an $^{0,3}A$ cross-ring cleavage ion formed by fragmentation of the mannose residue and which appeared at 59 mass units above the mass of the substituents linked to the mannose (*m/z* 262 for a GlcNAc-containing antenna and *m/z* 424 for Gal-GlcNAc, see Fig. 5).

Complex glycans

Representative spectra are shown in Fig. 6. Bi-, tri- and tetra-antennary glycans were found, with and without core fucose and with and without a bisecting GlcNAc residue. Exoglycosidase digestion with ABS, BTG and GUH (Fig. 2) showed that the antennae consisted of galactose and GlcNAc only. Their negative ion MS/MS spectra were identical to those from reference standards. The branching structure of the triantennary glycan (**29**, Fig. 6c) was revealed by the mass of the E_3 ion (*m/z* 831, the subscript "3" indicates its origin from the 3-antenna) (Harvey, 2005c; Harvey et al., 2008a). This ion was also present in the spectrum of the tetra-antennary glycan (**34**, Fig. 6d) but, whereas the D and $[D-18]^-$ ions from the 6-antenna in the spectrum of the triantennary glycan were at the same *m/z* values (688 and 670 respectively) as in the spectrum of the biantennary glycan (Fig. 6a), they moved to *m/z* 1053 and 1035 in the spectrum of the tetra-antennary glycan reflecting the presence of the additional Gal-GlcNAc moiety in the 6-antenna. An additional $[D-36]^-$ ion at *m/z* 1017 was also characteristic of this branched structure on the 6-antenna. The fucose substitution pattern on the core GlcNAc residue was defined by the masses of the $^{2,4}A_R$, $^{2,4}A_{R-1}$ and B_{R-1} ions as described above. The occurrence of a bisecting GlcNAc residue was determined by the presence of an abundant $[D-221]^-$ ion (e.g., *m/z* 670 in Fig. 6b), equivalent in mass to the $[M-18]^-$ ion from the corresponding compound that did not contain a bisecting GlcNAc residue, as described earlier (Harvey et al., 2008b).

These basic complex structures were accompanied by relatively large amounts of analogues with fewer numbers of galactose residues (Table 1), confirmed by incubations with bovine testis β-galactosidase. Four representative spectra are shown in Fig. 7. All illustrated compounds contain a fucose residue attached to the core GlcNAc as shown by the masses of the $^{2,4}A_R$, $^{2,4}A_{R-1}$ and B_{R-1} ions as above. The spectrum of the biantennary glycan lacking both galactose residues

Table 2
Percentages of various groups of *N*-glycan in SARS spike glycoprotein.

Glycan type		% Total
High-mannose	–	30
Hybrid	–	28
Complex	Total	42
	Biantennary	19
	Triantennary	12
	Tetraantennary	11
Truncated hybrid and complex (no galactose)	–	21

(**10**, Fig. 7a) contained D and $[D\text{-}18]^-$ ions at m/z 526 and 508, respectively, consistent with the absence of galactose in the 6-antenna. The C_1 ion was at m/z 220 showing GlcNAc at the non-reducing terminus. Addition of one galactose residue (Fig. 7b) produced a mixed spectrum of glycans with the galactose attached to either antenna (**15**) as shown by the two pairs of D and $[D\text{-}18]^-$ ions at m/z 526/508 (major isomer) and at m/z 688/670. Two C_1 ions at m/z 179 and 220 confirmed both hexose (galactose) and GlcNAc, respectively, at the non-reducing terminus. The $^{1,3}A_3$ ion at m/z 424 was consistent with the presence of a Gal-GlcNAc-containing antenna.

Most of the other spectra from the glycans containing low galactose were of mixtures. They were interpreted by postulation of the expected ions, based on the structures of the identified fully galactosylated compounds and finding the relevant diagnostic ions in the spectra. Thus, the spectrum of the compounds having the composition $Man_3GlcNAc_5Fuc_1$ (**17**, Fig. 7c) would be expected to contain contributions from the bisected biantennary glycan and the triantennary glycan, both lacking galactose. The spectrum contained a prominent ion at m/z 507 at the expected mass of the E ion from the triantennary glycan lacking galactose and D and $[D\text{-}18]^-$ ions at m/z 526/508 from the 6-antenna. The enhanced relative abundance of the ion at m/z 508 suggested the presence of a small amount of the bisected biantennary glycan, this ion corresponding to $[D\text{-}221]^-$. The two compounds (**24**) producing the spectrum in Fig. 7d were the degalactosylated tetra-antennary glycan and the bisected triantennary compound. The former compound produced the characteristic D, $[D\text{-}18]^-$ and $[D\text{-}36]^-$ triplet at m/z 729, 711 and 693 from the 6-antenna and the E ion at m/z 507. The other, minor compound was characterized by the $[D\text{-}221]^-$ ion at m/z 508. The ion corresponding to the antenna mass plus 59 mass units ($C_2H_3O_2$ from the attached mannose) also defined the antenna composition (the specific cross-ring cleavage producing these A-type ions varied with the linkage position of the antenna).

Effect of NB-DNJ treatment

Effect of NB-DNJ against SARS-CoV infection

Following infection with SARS-CoV (strain Tor2, MOI = 10^{-4}) and incubation with the iminosugar inhibitor *N*B-DNJ, the integrity of the Vero E6 cell monolayer was monitored daily by light microscopy. At *N*B-DNJ concentrations of 100 μg/mL and above, the cell monolayer remained intact and showed no signs of virally-induced cytopathic effects (CPE). However, no significant toxicity was seen at this drug concentration as shown by the XTT assay (data not shown).

Effect of NB-DNJ treatment on N-glycan profiles

Fig. 8b shows the NP-HPLC profile of the *N*-glycans from the spike protein that was obtained in the presence of *N*B-DNJ at 100 μg/mL, the concentration that protected the cells against CPE. The glycans of higher molecular weight than were observed in the sample without *N*B-DNJ were identified by HPLC and exoglycosidase digestion (*A. ureafaciens* sialidase, bovine testis β-galactosidase *S. pneumonia N*-acetyl-hexosaminidase, Jack bean α-mannosidase and bovine kidney α-fucosidase) as $Glc_3Man_7GlcNAc_2$, $Glc_3Man_8GlcNAc_2$ and $Glc_3Man_9GlcNAc_2$ showing that *N*B-DNJ at the concentration used (100 μg/mL) was able to

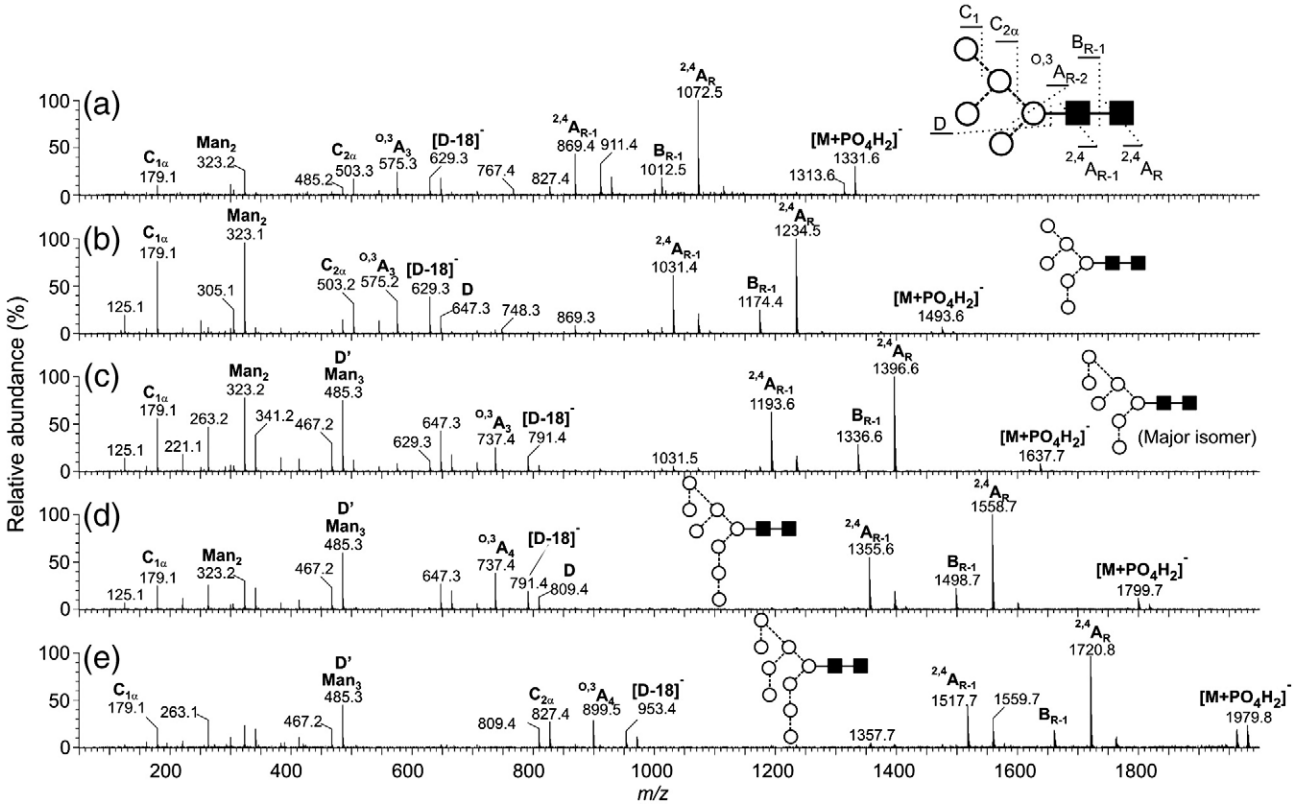

Fig. 4. Negative ion MS/MS spectra of the $[M+H_2PO_4]^-$ ions from the high-mannose glycans $Man_{5-9}GlcNAc_2$. Symbols for the structural diagrams are defined in the legend to Fig. 2. Ions are labelled according to the scheme introduced by Domon and Costello (1988).

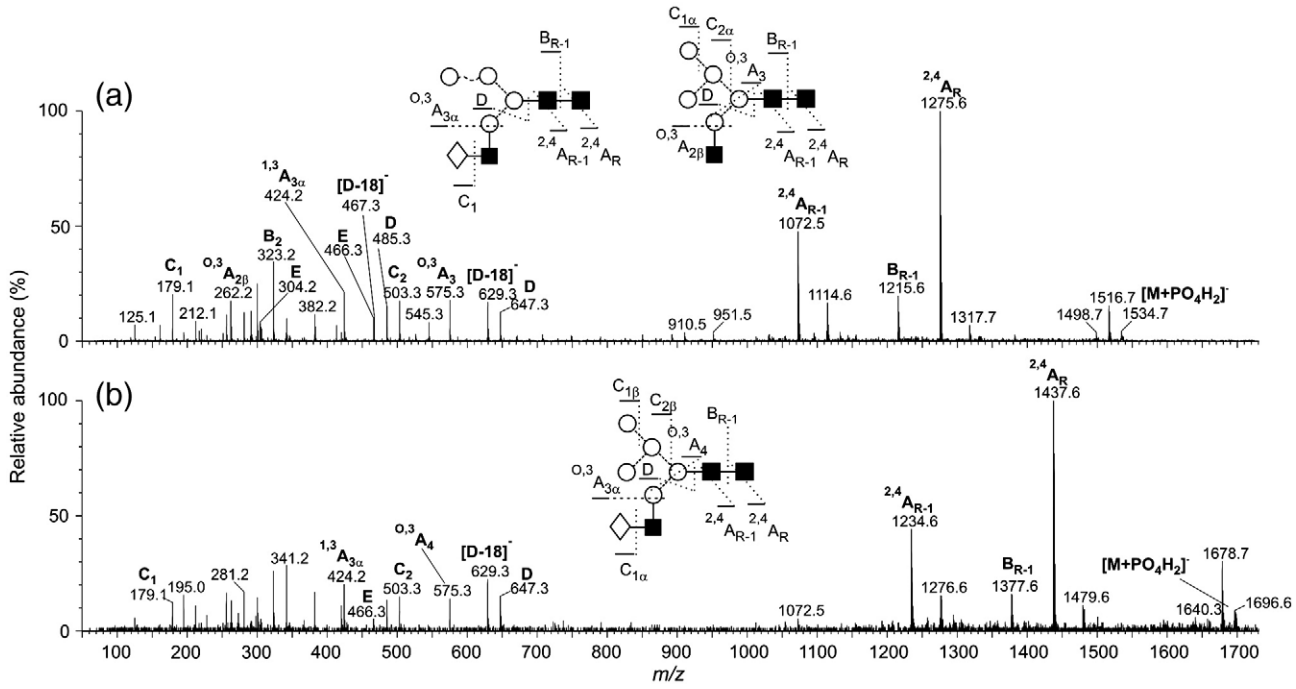

Fig. 5. Negative ion MS/MS spectra of the $[M+H_2PO_4]^-$ ions from the hybrid glycans **9** and **14**. Symbols for the structural diagrams are defined in the legend to Fig. 2.

partially inhibit glycan processing by blocking the first stage, namely removal of the terminal glucose residues from the 3-antenna. α-Mannosidase was, however, still able to remove the outer mannose residues from the 6-antenna to give the observed compounds. Although processing of the 3-antenna was blocked, complex glycans were still found in the profile. The most likely reason would be the presence of an *endo*-mannosidase that was able to split off Glc_3Man from the 3-antenna. Such an enzyme has been reported from rats

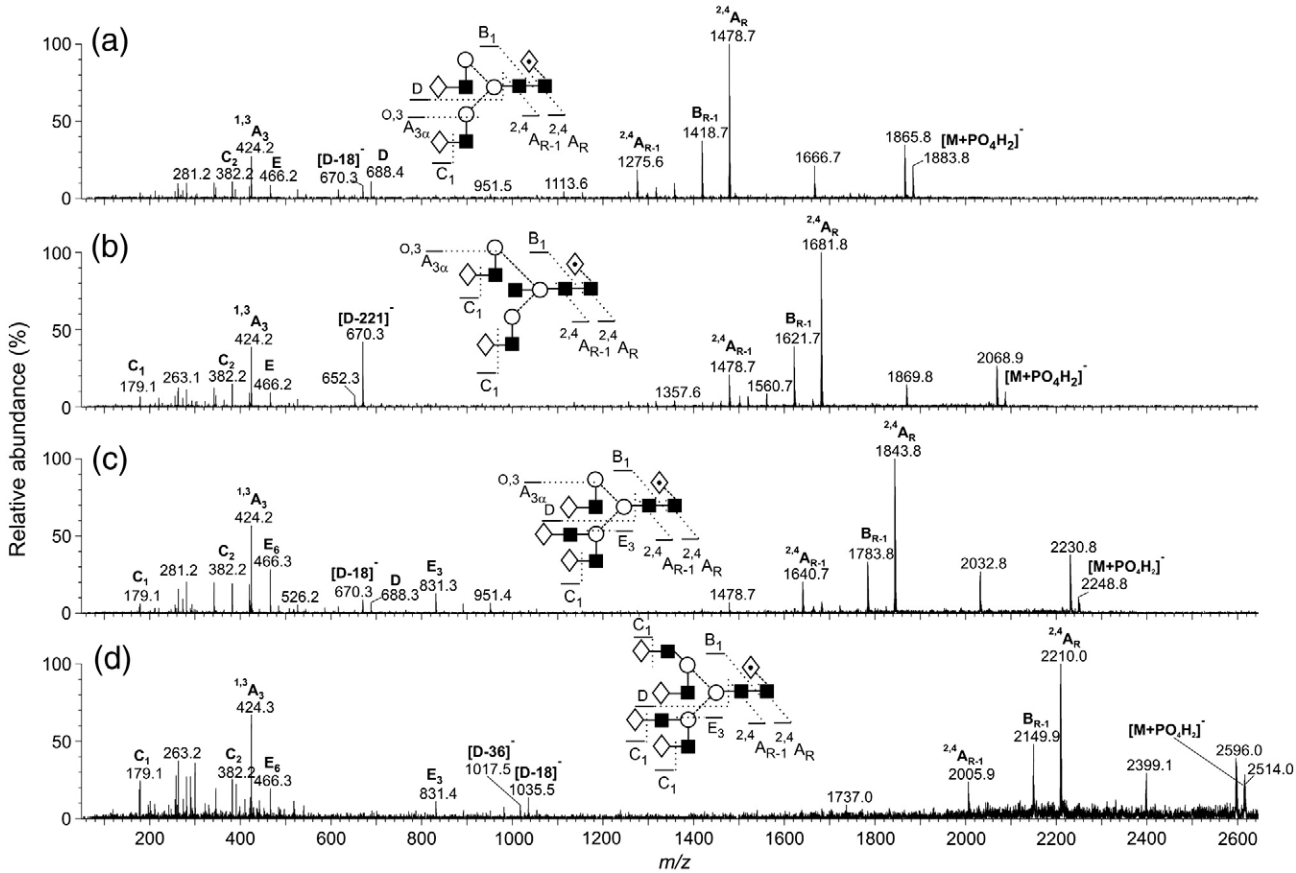

Fig. 6. Negative ion MS/MS spectra of the $[M+H_2PO_4]^-$ ions from (a) the fucosylated biantennary glycan **21**, (b) the bisected, fucosylated biantennary glycan **26**, (c) the fucosylated triantennary glycan **29** and (d) the fucosylated tetra-antennary glycan **34**. Symbols for the structural diagrams are defined in the legend to Fig. 2.

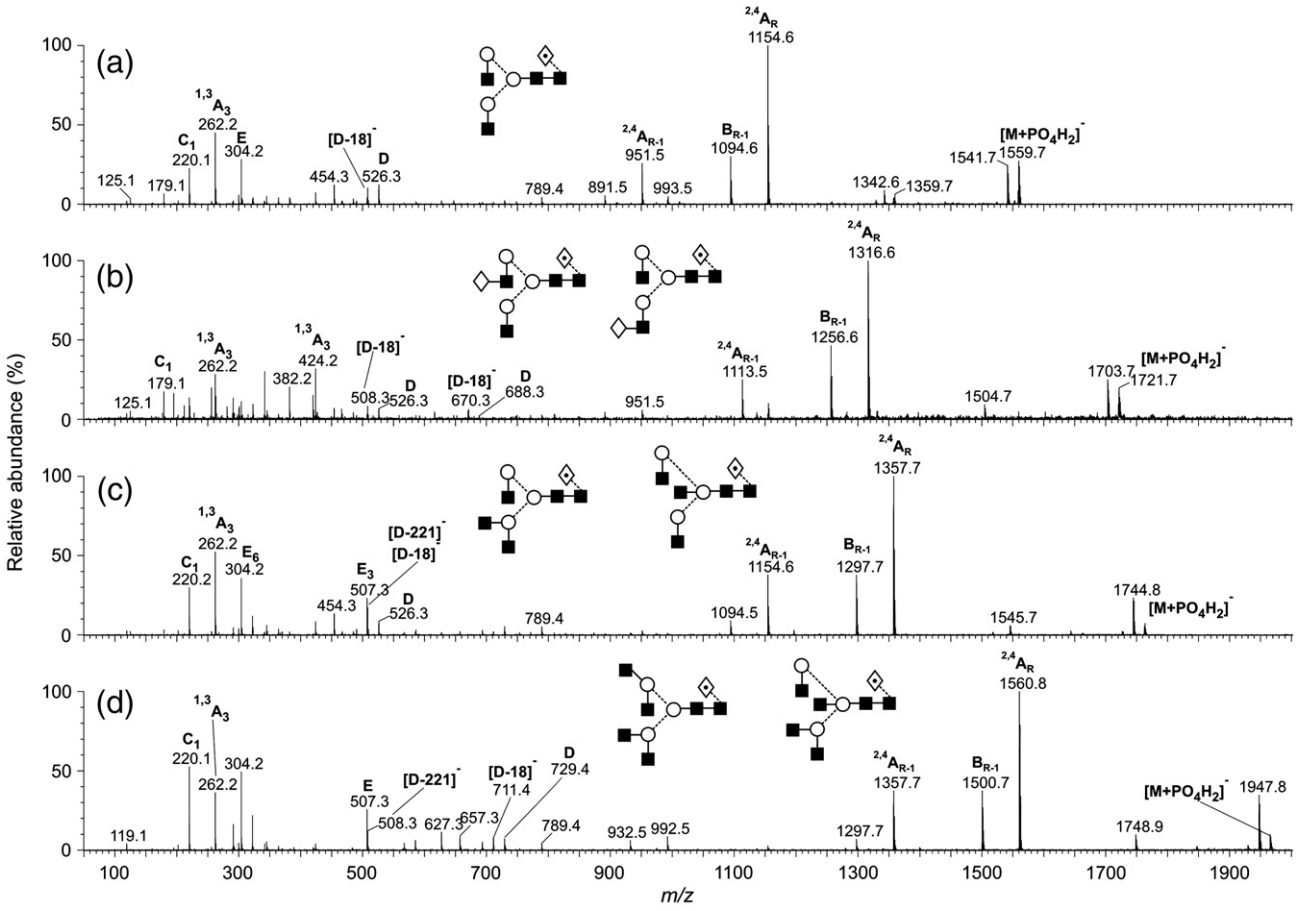

Fig. 7. Negative ion MS/MS spectra of the $[M+H_2PO_4]^-$ ions from (a) the fucosylated biantennary glycan lacking galactose (**10**), (b) a mixture of the fucosylated biantennary glycan with one galactose residue on either antenna (**15**), (c) a mixture of the fucosylated triantennary glycan and the bisected biantennary glycan lacking galactose (**17**) and (d) a mixture of the fucosylated tetra-antennary glycan and the bisected triantennary glycan lacking galactose (**24**). Symbols for the structural diagrams are defined in the legend to Fig. 2.

(Lubas and Spiro, 1987; Lubas and Spiro, 1988; Moore and Spiro, 1990) but there appears to be no information on its possible occurrence in the African green monkey. However, the high abundance of the peak labelled as 29 in Fig. 8b is accounted for by the isomer of $Man_8GlcNAc_2$ that has lost a mannose residue from the 3-antenna (same GU value as the fucosylated triantennary glycan) supporting this proposal.

Although the postulated endomannosidase activity permits extensive *N*-glycan processing with the production of complex glycans and a nearly normal profile in the presence of *N*B-DNJ, the drug prevents formation of the mono-glucosylated *N*-glycans that are necessary for binding to the chaperones calnexin and calreticulin that are essential for correct protein folding. Viral surface glycoproteins are dependent on such an interaction for correct folding (Vigerust and Shepherd, 2007). Thus, α-glucosidase inhibition will prevent this interaction and potentially lead to regional or global glycoprotein misfolding. Therefore, the observation that the SARS-CoV S glycoprotein can undergo extensive *N*-glycan processing to complex structures in the presence of *N*B-DNJ does not necessarily correlate with proper glycoprotein folding. Unfortunately, the necessary conformationally sensitive anti-SARS-CoV S antibodies for testing this conclusion were not available at the time this study was performed. Improper folding induced by *N*B-DNJ could explain the protective effect of the drug towards viral infection but the ability to retain complex *N*-glycan processing could contribute to the drug's low cytotoxicity.

Conclusions

This study is the first to describe fully the range of *N*-glycans present on the SARS-CoV spike glycoprotein. They consisted mainly of high-mannose ($Man_{5-9}GlcNAc_2$, about 30% of the total glycans), hybrid (28%) and bi-, tri- and tetra-antennary complex glycans (42%) with and without both bisecting GlcNAc and core fucose. Complex glycans with fewer than the full complement of galactose residues were present in relatively high abundance with 49% of the complex glycans carrying no galactose. Sialylation was negligible. No evidence was found for glycans with *N*-acetyllactosamine extensions or with fucose attached to an antenna. The relatively high abundance of

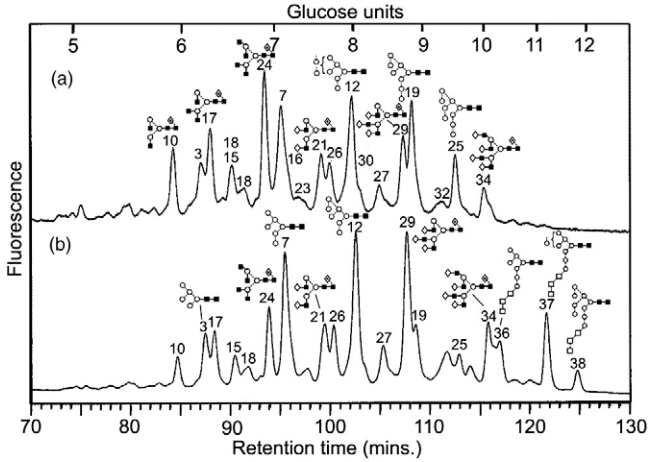

Fig. 8. (a) NP-HPLC analysis of SARS-CoV *N*-glycans obtained without (a) and with (b) 100 μg/mL *N*B-DNJ. Peaks are identified in Table 1. The three glycans with residual glucose residues are highlighted.

complex glycans lacking one or more of the normal galactose residues might indicate the involvement of the lectin, LSECtin in viral binding, as recently found for Ebola virus (Powlesland et al., 2008).

Treatment with the glucosidase inhibitor *N*B-DNJ inhibited *N*-glycan processing as evidenced by the appearance in the profiles of glycans of composition $Glc_3Man_{7-9}GlcNAc_2$. However, some complex glycans still appeared in the glycan profile, suggesting the presence of an α-endomannosidase that was able to hydrolyse the Glc_3-Man_3 chain of the 3-antenna allowing attachment of GlcNAc in the first step towards complex glycan biosynthesis. Protection of cells against the cytopathic effects of the virus, possibly as the result of the inhibition of glycan processing, suggests a possible use of glucosidase inhibitors to treat SARS-CoV infections.

Materials and methods

Materials

Methanol was obtained from BDH Ltd. (Poole, UK). Ammonium phosphate and 2,5-dihydroxybenzoic acid (DHB) were from Aldrich Chemical Co. Ltd. (Poole); water was distilled before use in a quartz apparatus. *N*B-DNJ was a gift from Monsanto Searle (St Louis, USA).

Preparation of SARS-CoV

All work with infectious SARS-CoV was performed in the high biocontainment laboratory of the National Microbiology Laboratory (NML) of the Public Health Agency of Canada (PHAC). Vero E6 cells (ATCC CRL-1586, kidney epithelial cells derived from African green monkeys (*Cercopithecus aethiops*)) were cultured in Dulbecco's modified Eagle's medium (DMEM) containing 10% fetal bovine serum (FBS) and subsequently infected with the Tor2 strain of the SARS-CoV (Marra et al., 2003) at an MOI of 10^{-4} with and without the presence of different concentrations (0, 100, 500 and 1000 mg/mL) of *N*B-DNJ. After 1 h of virus adsorption, cells were washed 3 times and DMEM supplemented with 2% FBS (with and without *N*B-DNJ) was added. Forty-eight hours post-infection, the cell supernatant was harvested and cells were cleared by low-speed centrifugation. Virus particles were pelleted through a 20% sucrose cushion at 20,000 rpm for 2 h, washed with PBS and resuspended and inactivated in 1× sample loading buffer with 1.5% SDS. Infectivity was further inactivated by heating the specimens at 100 °C for 15 min prior to removal from high biocontainment.

Assay for cellular toxicity

Vero E6 cells were cultured in 96-well plates in DMEM supplemented with 10% FBS. At 80% confluency the medium was removed and replaced with DMEM/2% FBS containing various concentrations (10–1000 μg/mL) of *N*B-DNJ, 5 wells per each concentration. Drug cytotoxicity was assessed on days 1, 2 and 3 post-treatment using the XTT metabolic assay (Roche, Laval, Canada) according to the manufacturer's directions.

SDS-PAGE analysis of SARS-CoV preparation

The SARS-CoV preparation was analysed by 9% polyacrylamide gel electrophoresis (SDS-PAGE) followed by Coomassie blue staining. The stained protein band corresponding to the SARS-CoV S glycoprotein was cut from the gel for enzymatic digestion with peptide *N*-glycosidase F (PNGase F, Roche Diagnostics Ltd., Basel, Switzerland) and subsequent *N*-glycan analysis (see below).

Western blotting analysis of the SARS-CoV S glycoprotein

To confirm that the band selected for *N*-glycan analysis was that corresponding to the SARS-CoV S glycoprotein, an anti-SARS-CoV S antibody was used in a western blotting protocol. Briefly, the SARS-CoV preparation was subjected to SDS-PAGE on a 9% gel and the proteins were transferred to PVDF membranes using the semi-dry transfer technique. The membranes were blocked in 5% milk solution in 1× phosphate-buffered saline (PBS) overnight then incubated with a mouse anti-SARS IgG1 (clone 16F1071, Imgenex, CA, USA) diluted 1:1000 in 3% milk solution at room temperature for at least 1 h. The membranes were washed three times in PBS–0.05% Tween-20 before 1 h incubation at room temperature with a horseradish peroxidase (HRP)-conjugated goat anti-mouse secondary antibody (Sigma Chemicals) diluted 1:1000 in 3% milk solution. The membranes were washed three times in PBS–0.05% Tween-20, then once with PBS. The SARS-CoV glycoprotein band was detected by developing the membranes using the ECL Western blotting detection kit (Amersham Biosciences, Little Chalfont, UK) according to the manufacturers instructions and followed by exposure to X-ray film (CL-X Posure film, Pierce).

N-glycan release using peptide N-glycosidase F

The procedure essentially followed that described by Küster et al. (1997). The glycoproteins were separated by SDS-PAGE with a BioRad Mini-Protean II apparatus with 80×80×0.75 mm plates and a 9% resolving gel. Developed gels were stained with Coomassie Blue R-250. The SARS-CoV S glycoprotein gel bands were excised from the gel and cut into pieces about 1 mm^2, washed with 300 μL 20 mM $NaHCO_3$ (BDH Limited, Poole, UK) and soaked in the buffer for 30 min. This procedure was repeated twice; on the third wash, 45 mM dithiothreitol (20 μL) was added and incubated for 30 min at 60 °C to reduce disulfide bonds. Iodoacetamide (100 mM; 20 μL) was added and the solution was incubated for 30 min in the dark. Then a 1:1 (v/v) solution (300 μL) of aqueous acetonitrile:20 mM $NaHCO_3$, pH 7.0, was added and incubated for 60 min followed by vacuum drying. PNGase F (EC 3.2.2.18, 30 mL, 100 U/mL; Roche Diagnostics Ltd.) and $NaHCO_3$ buffer (enough to cover the gel, 70–100 μL) was added to the dried gel pieces which were incubated at 37 °C for 12–16 h (overnight). The supernatant was retained and the gel was washed twice with water (200 μL), and then with acetonitrile (200 μL, Riedel de Häen Laboratory, Seelze, Germany); the washes were collected and desalted by incubation with 50 μL H^+-activated AG-50, then centrifuged. The supernatant was filtered through 0.45 μm Millipore LH hydrophilic PTFE syringe-tip filter then vacuum dried in preparation for direct mass spectrometric analysis or 2-aminobenzamide (2AB) labelling followed by HPLC analysis. Samples for mass spectrometric analysis were further cleaned by drop dialysis with a Nafion 117 membrane (Börnsen et al., 1995).

Glycan derivatisation with 2-aminobenzamide

Glycans were labelled with 2AB by reductive amination (Bigge et al., 1995) using a 2AB labelling kit from Glyko (now part of Prozyme at Hayward, CA, USA). The 2AB labelling solution was prepared according to the manufacturer's instructions and stored at −20 °C. Five microliters of this solution was added to the dried sugars and incubated at 65 °C for 2 h. Residual 2AB reagent was removed by ascending paper chromatography on 3MM chromatography paper (Millipore, Watford, UK) in 100% acetonitrile. After 2 h, the sample was viewed under a UV light and the spot corresponding to the labelled sugars was cut from the paper and the sugars were eluted using four sequential aliquots of water (0.5 mL) into a nitric acid-washed glass tube. The eluted *N*-glycans were vacuum dried and then redissolved in water (200 μL).

Glycan sequencing using exoglycosidase digestion

One to two picomoles of 2AB-labelled *N*-glycans were vacuum dried and incubated at 37 °C for 10 h in 50 mM sodium citrate

buffer (pH 5.2) with exoglycosidases (Glyko) as follows: *Arthrobacter ureafaciens* sialidase (ABS, EC 3.2.1.18), a mixture of ABS and bovine testis β-galactosidase (BTG, EC 3.2.1.23), and a mixture of ABS, BTG and *Streptococcus pneumoniae N*-acetyl-hexosaminidase (GUH, EC 3.2.1.30) at the manufacturer's recommended concentrations. In a second experiment, glycans were incubated with Jack bean mannosidase (JBM, EC 3.2.1.24) 10 μL, 50 U/mL and *Aspergillus saitoi* α1-2-mannosidase (ASM), 2 μL, 1 mU/mL. The enzymes were removed after exoglycosidase digestions using washed (200 μL water, centrifugation at 7000 rpm for 10 min) nitrocellulose 0.45 μm microspin filters (Radleys, Saffron Walden, UK). The sample (10 μL) was added to the filter and centrifuged at 13,000 rpm for 3 min. The digestion tube was washed with water (20 μL) which was transferred to the filter and centrifuged at 13,000 rpm for 3 min. The filter was rinsed with water (100 μL) and centrifuged at 13,000 rpm for a further 3 min. The collected solution was vacuum dried and then redissolved in water (20 μL) for analysis by HPLC.

Normal-phase HPLC analysis

Acetonitrile (80 μL) was added to 10% of the sample (20 μL) and 95 μL was examined on a normal-phase (NP)-HPLC system (Waters Alliance 2690, Waters Corporation, Milford, MA, USA) fitted with a GlycoSep N column (Oxford GlycoSciences, Abingdon, UK) with a run time of 180 min (Guile et al., 1996). The *N*-linked sugars eluted from the column with a retention time of between 40 and 120 min. Comparison with a dextran ladder allowed assignment of glucose unit (GU) values to each peak, which facilitated identification of the glycans present in the released pool.

Matrix-assisted laser desorption/ionization time-of-flight mass spectrometry (MALDI-TOF MS)

Positive ion MALDI-TOF mass spectra were obtained with a Waters-MS Technologies TofSpec 2E reflectron TOF mass spectrometer (Waters Ltd, Manchester). The pulse and acceleration voltages were 3 and 20 kV, respectively. Data acquisition and processing were performed with MassLynx software version 3.3. Samples were prepared by mixing an aqueous solution of the sample (0.5 μL) with a saturated solution of DHB in acetonitrile (0.3 μL) on the stainless steel MALDI target and allowing the mixture to dry under ambient conditions. The dried sample spot was then re-dissolved in ethanol (0.2 μL) and again allowed to dry.

Electrospray mass spectrometry

Electrospray mass spectrometry was performed with a Waters quadrupole-time-of-flight (Q-TOF) Ultima Global instrument in negative ion mode. Samples in 1:1 (v:v) methanol:water were infused through Proxeon nanospray capillaries (Proxeon Biosystems, Odense, Denmark). The ion source conditions were as follows: temperature, 120 °C; nitrogen flow, 50 L/h; infusion needle potential, 1.2 kV; cone voltage, 100 V; RF-1 voltage, 150 V. Spectra (2 s scans) were acquired with a digitization rate of 4 GHz and accumulated until a satisfactory signal:noise ratio had been obtained. The major ions were $[M+H_2PO_4]^-$, the phosphate apparently arising from residual phosphate in the original sample, as observed previously from all glycan samples released as above. For MS/MS data acquisition, the parent ion was selected at low resolution (about 5 m/z mass window) to allow transmission of isotope peaks and fragmented with argon at a pressure (recorded on the instrument's pressure gauge) of 0.5 mBar. The voltage on the collision cell was adjusted with mass and charge to give an even distribution of fragment ions across the mass scale. Typical values were 80–120 V. Other voltages were as recommended by the manufacturer. Instrument control, data acquisition and processing were performed with MassLynx software version 4.0. Displayed spectra have been smoother using the Savitzky Golay algorithm (5×2) and abundant background ions at m/z 195, 291 and 344 have been removed for clarity.

Acknowledgments

We thank the Wellcome Trust and the Biotechnology and Biological Sciences Research Council for equipment grants to purchase the Q-TOF and TofSpec mass spectrometers, respectively. We thank the Public Health Agency of Canada (PHAC) for financial support.

References

Bergeron, E., Vincent, M.J., Wickham, L., Hamelin, J., Basak, A., Nichol, S.T., Chrétien, M., Seidah, N.G., 2005. Implication of proprotein convertases in the processing and spread of severe acute respiratory syndrome coronavirus. Biochem. Biophys. Res. Commun. 326, 554–563.

Bigge, J.C., Patel, T.P., Bruce, J.A., Goulding, P.N., Charles, S.M., Parekh, R.B., 1995. Nonselective and efficient fluorescent labeling of glycans using 2-aminobenzamide and anthranilic acid. Anal. Biochem. 230, 229–238.

Börnsen, K.O., Mohr, M.D., Widmer, H.M., 1995. Ion exchange and purification of carbohydrates on a Nafion(R) membrane as a new sample pretreatment for matrix-assisted laser desorption-ionization mass spectrometry. Rapid Commun. Mass Spectrom. 9, 1031–1034.

Chen, J., Subbarao, K., 2007. The immunobiology of SARS. Annu. Rev. Immunol. 25, 443–472.

Domon, B., Costello, C.E., 1988. A systematic nomenclature for carbohydrate fragmentations in FAB-MS/MS spectra of glycoconjugates. Glycoconj. J. 5, 397–409.

Drosten, C., Günther, S., Preiser, W., van der Werf, S., Brodt, H.-R., Becker, S., Rabenau, H., Panning, M., Kolesnikova, L., Fouchier, R.A.M., Berger, A., Burguière, A.-M., Cinatl, J., Eickmann, M., Escriou, N., Grywna, K., Kramme, S., Manuguerra, J.-C., Müller, S., Rickerts, V., Stürmer, M., Vieth, S., Klenk, H.-D., Osterhaus, A.D.M.E., Schmitz, H., Doerr, H.W., 2003. Identification of a novel coronavirus in patients with severe acute respiratory syndrome. New Eng. J. Med. 348, 1967–1976.

Eickmann, M., Becker, S., Klenk, H.D., Doerr, H.W., Stadler, K., Censini, S., Guidotti, S., Masignani, V., Scarselli, M., Mora, M., Donati, C., Han, J.H., Song, H.C., Abrignani, S., Covacci, A., Rappuoli, R., 2003. Phylogeny of the SARS coronavirus. Science 302, 1504–1505.

Feldmann, H., Nichol, S.T., Klenk, H.D., Peters, C.J., Sanchez, A., 1994. Characterization of filoviruses based on differences in structure and antigenicity of the virion glycoprotein. Virology 199, 469–473.

Follis, K.E., York, J., Nunberg, J.H., 2006. Furin cleavage of the SARS coronavirus spike glycoprotein enhances cell–cell fusion but does not affect virion entry. Virology 350, 358–369.

Guile, G.R., Rudd, P.M., Wing, D.R., Prime, S.B., Dwek, R.A., 1996. A rapid high-resolution high-performance liquid chromatographic method for separating glycan mixtures and analyzing oligosaccharide profiles. Anal. Biochem. 240, 210–226.

Han, D.P., Lohani, M., Cho, M.W., 2007. Specific asparagine-linked glycosylation sites are critical for DC-SIGN- and L-SIGN-mediated severe acute respiratory syndrome coronavirus entry. J. Virol. 81, 12029–12039.

Harvey, D.J., 2005a. Fragmentation of negative ions from carbohydrates. Part 1. Use of nitrate and other anionic adducts for the production of negative ion electrospray spectra from *N*-linked carbohydrates. J. Am. Soc. Mass Spectrom. 16, 622–630.

Harvey, D.J., 2005b. Fragmentation of negative ions from carbohydrates. Part 2. Fragmentation of high-mannose *N*-linked glycans. J. Am. Soc. Mass Spectrom. 16, 631–646.

Harvey, D.J., 2005c. Fragmentation of negative ions from carbohydrates. Part 3. Fragmentation of hybrid and complex *N*-linked glycans. J. Am. Soc. Mass Spectrom. 16, 647–659.

Harvey, D.J., Martin, R.L., Jackson, K.A., Sutton, C.W., 2004. Fragmentation of *N*-linked glycans with a MALDI-ion trap time-of-flight mass spectrometer. Rapid Commun. Mass Spectrom. 18, 2997–3007.

Harvey, D.J., Crispin, M., Scanlan, C., Singer, B.B., Lucka, L., Chang, V.T., Radcliffe, C.M., Thobhani, S., Yuen, C.-T., Rudd, P.M., 2008a. Differentiation between isomeric triantennary N-linked glycans by negative ion tandem mass spectrometry and confirmation of glycans containing galactose attached to the bisecting (β1-4-GlcNAc) residue in *N*-glycans from IgG. Rapid Commun. Mass Spectrom. 22, 1047–1052.

Harvey, D.J., Royle, L., Radcliffe, C.M., Rudd, P.M., Dwek, R.A., 2008b. Structural and quantitative analysis of *N*-linked glycans by MALDI and negative ion nanospray mass spectrometry. Anal. Biochem. 376, 44–60.

Harvey, D.J., Merry, A.H., Royle, L., Campbell, M.P., Dwek, R.A., Rudd, P.M., 2009. Proposal for a standard system for drawing structural diagrams of *N*- and *O*-linked carbohydrates and related compounds. Proteomics 9, 3796–3801.

Jeffers, S.A., Tusell, S.M., Gillim-Ross, L., Hemmila, E.M., Achenbach, J.E., Babcock, G.J., Thomas, W.D.J., Thackray, L.B., Young, M.D., Mason, R.J., Ambrosino, D.M., Wentworth, D.E., DeMartini, J.C., Holmes, K.V., 2004. CD209L (L-SIGN) is a receptor for severe acute respiratory syndrome coronavirus. Proc. Natl. Acad. Sci., USA 101, 15748–15753.

Krokhin, O., Li, Y., Andonov, A., Feldmann, H., Flick, R., Jones, S., Stroeher, U., Bastien, N., Dasuri, K.V.N., Cheng, K., Simonsen, J.N., Perreault, H., Wilkins, J., Ens, W., Plummer, F., Standing, K.G., 2003. Mass spectrometric characterization of proteins from the SARS virus. A preliminary report. Mol. Cell. Proteomics 2, 346–356.

Ksiazek, T.G., Erdman, D., Goldsmith, C.S., Zaki, S.R., Peret, T., Emery, S., Tong, S., Urbani, C., Comer, J.A., Lim, W., Rollin, P.E., Dowell, S.F., Ling, A.-E., Humphrey, C.D., Shieh, W.-J., Guarner, J., Paddock, C.D., Rota, P., Fields, B., DeRisi, J., Yang, J.-Y., Cox, N., Hughes, J.M., LeDuc, J.W., Bellini, W.J., Anderson, L.J., Cannon, A.D.L., Curtis, M., Farrar, B., Morgan, L., Pezzanite, L., Sanchez, A.J., Slaughter, K.A., Stevens, T.L., Stockton, P.C., Wagoner, K.D., Sanchez, A., Nichol, S., Vincent, M., Osborne, J., Honig, J., Erickson, B.R., Holloway, B., McCaustland, K., Lingappa, J., Lowe, L., Scott, S., Lu, X., Villamarzo, Y., Cook, B., Chen, Q., Birge, C., Shu, B., Pallansch, M., Tatti, K.M., Morken, T., Smith, C., Greer, P., White, E., McGlothen, T., Bhatnagar, J., Patel, M., Bartlett, J., Montague, J., Lee, W., Packard, M., Thompson, H.A., Moen, A., Fukuda, K., Uyeki, T., Harper, S., Klimov, A., Lindstrom, S., Benson, R., Carlone, G., Facklam, R., Fields, P., Levett, P., Mayer, L., Talkington, D., Thacker, W.L.T., Tondella, M.L.C., Whitney, C., Robertson, B., Warnock, D., Brooks, J.T., Schrag, S., Rosenstein, N., Ganem, D., Poutanen, S.M., Chen, T.-J., Hsiao, C.-H., Wai-Fu, N.G., Ho, M., Keung, T.-K., Nghiem, K.H., Nguyen, H.K.L., Le, M.Q., Nguyen, H.H.T., Hoang, L.T., Vu, T.H., Vu, H.Q., Chunsuttiwat, S., 2003. A novel coronavirus associated with severe acute respiratory syndrome. New Eng. J. Med. 348, 1953–1966.

Küster, B., Wheeler, S.F., Hunter, A.P., Dwek, R.A., Harvey, D.J., 1997. Sequencing of *N*-linked oligosaccharides directly from protein gels: in-gel deglycosylation followed by matrix-assisted laser desorption/ionization mass spectrometry and normal-phase high performance liquid chromatography. Anal. Biochem. 250, 82–101.

Li, W., Moore, M.J., Vasilieva, N., Sui, J., Wong, S.K., Berne, M.A., Somasundaran, M., Sullivan, J.L., Luzuriaga, K., Greenough, T.C., Choe, H., Farzan, M., 2003. Angiotensin-converting enzyme 2 is a functional receptor for the SARS coronavirus p450. Nature 426, 450–454.

Li, F., Li, W., Farzan, M.F., Harrison, S.C., 2005. Structure of SARS coronavirus spike receptor-binding domain complexed with receptor. Science 309, 1864–1868.

Lubas, W.A., Spiro, R.G., 1987. Golgi endo-alpha-D-mannosidase from rat liver, a novel *N*-linked carbohydrate unit processing enzyme. J. Biol. Chem. 262, 3775–3781.

Lubas, W.A., Spiro, R.G., 1988. Evaluation of the role of rat liver Golgi endo-alpha-D-mannosidase in processing *N*-linked oligosaccharides. J. Biol. Chem. 263, 3990–3998.

Marra, M.A., Jones, S.J.M., Astell, C.R., Holt, R.A., Brooks-Wilson, A., Butterfield, Y.S.N., Khattra, J., Asano, J.K., Barber, S.A., Chan, S.Y., Cloutier, A., Coughlin, S.M., Freeman, D., Girn, N., Griffith, O.L., Leach, S.R., Mayo, M., McDonald, H., Montgomery, S.B., Pandoh, P.K., Petrescu, A.S., Robertson, A.G., Schein, J.E., Siddiqui, A., Smailus, D.E., Stott, J.M., Yang, G.S., Plummer, F., Andonov, A., Artsob, H., Bastien, N., Bernard, K., Booth, T.F., Bowness, D., Czub, M., Drebot, M., Fernando, L., Flick, R., Garbutt, M., Gray, M., Grolla, A., Jones, S., Feldmann, H., Meyers, A., Kabani, A., Li, Y., Normand, S., Stroher, U., Tipples, G.A., Tyler, S., Vogrig, R., Ward, D., Watson, B., Brunham, R.C., Krajden, M., Petric, M., Skowronski, D.M., Upton, C., Roper, R.L., 2003. The genome sequence of the SARS-associated coronavirus. Science 300, 1399–1404.

Marzi, A., Gramberg, T., Simmons, G., Möller, P., Rennekamp, A.J., Krumbiegel, M., Geier, M., Eisemann, J., Turza, N., Saunier, B., Steinkasserer, A., Becker, S., Bates, P., Hofmann, H., Pöhlmann, S., 2004. DC-SIGN and DC-SIGNR interact with the glycoprotein of Marburg virus and the S protein of severe acute respiratory syndrome coronavirus. J. Virol. 78, 12090–12095.

Moore, S.E., Spiro, R.G., 1990. Demonstration that Golgi endo-alpha-D-mannosidase provides a glucosidase-independent pathway for the formation of complex *N*-linked oligosaccharides of glycoproteins. J. Biol. Chem. 265, 13104–13112.

Moore, M.J., Dorfman, T., Li, W., Wong, S.K., Li, Y., Kuhn, J.H., Coderre, J., Vasilieva, N., Han, Z., Greenough, T.C., Farzan, M., Choe, H., 2004. Retroviruses pseudotyped with the severe acute respiratory syndrome coronavirus spike protein efficiently infect cells expressing angiotensin-converting enzyme 2. J. Virol. 78, 10628–10635.

Powlesland, A.S., Fisch, T., Taylor, M.E., Smith, D.F., Tissot, B., Dell, A., Pohlmann, S., Drickamer, K., 2008. A novel mechanism for LSECtin binding to Ebola virus surface glycoprotein through truncated glycans. J. Biol. Chem. 283, 593–602.

Rota, P.A., Oberste, M.S., Monroe, S.S., Nix, W.A., Campagnoli, R., Icenogle, J.P., Penaranda, S., Bankamp, B., Maher, K., Chen, M.-h., Tong, S., Tamin, A., Lowe, L., Frace, M., DeRisi, J.L., Chen, Q., Wang, D., Erdman, D.D., Peret, T.C.T., Burns, C., Ksiazek, T.G., Rollin, P.E., Sanchez, A., Liffick, S., Holloway, B., Limor, J., McCaustland, K., Olsen-Rasmussen, M., Fouchier, R., Günther, S., Osterhaus, A.D.M.E., Drosten, C., Pallansch, M.A., Anderson, L.J., Bellini, W.J., 2003. Characterization of a novel coronavirus associated with severe acute respiratory syndrome. Science 300, 1394–1399.

Shi, Z., Hu, Z., 2008. A review of studies on animal reservoirs of the SARS coronavirus. Virus Res 133, 74–87.

Song, H.C., Seo, M.Y., Stadler, K., Yoo, B.J., Choo, Q.L., Coates, S.R., Uematsu, Y., Harada, T., Greer, C.E., Polo, J.M., Pileri, P., Eickmann, M., Rappuoli, R., Abrignani, S., Houghton, M., Han, J.H., 2004. Synthesis and characterization of a native oligomeric form of recombinant severe acute respiratory syndrome coronavirus spike glycoprotein. J. Virol. 78, 10328–10335.

Tan, Y.-J., Lim, S.G., Hong, W., 2006. Understanding the accessory viral proteins unique to the severe acute respiratory syndrome (SARS) coronavirus. Antiviral Res. 72, 78–88.

Tripet, B., Howard, M.W., Jobling, M., Holmes, R.K., Holmes, K.V., Hodges, R.S., 2004. Structural characterization of the SARS-coronavirus spike S fusion protein core. J. Biol. Chem. 279, 20836–20849.

Vigerust, D.J., Shepherd, V.L., 2007. Virus glycosylation: role in virulence and immune interactions. Trends Microbiol 15, 211–218.

Wang, L.F., Eaton, B.T., 2007. Bats, civets and the emergence of SARS. Curr. Top. Microbiol. Immunol. 315, 325–344.

Wang, P., Chen, J., Zheng, A., Nie, Y., Shi, X., Wang, W., Wang, G., Luo, M., Liu, H., Tan, L., Song, X., Wang, Z., Yin, X., Qu, X., Wang, X., Qing, T., Ding, M., Deng, H., 2004. Expression cloning of functional receptor used by SARS coronavirus. Biochem. Biophys. Res. Commun. 315, 439–444.

Wang, L.F., Shi, Z., Zhang, S., Field, H., Daszak, P., Eaton, B.T., 2006. Review of bats and SARS. Emerg. Infect. Dis. 12, 1834–1840.

Xiao, X., Chakraborti, S., Dimitrov, A.S., Gramatikoff, K., Dimitrov, D.S., 2003. The SARS-CoV S glycoprotein: expression and functional characterization. Biochem. Biophys. Res. Commun. 312, 1159–1164.

Yang, Z.-Y., Huang, Y., Ganesh, L., Leung, K., Kong, W.-P., Schwartz, O., Subbarao, K., Nabel, G.J., 2004. pH-dependent entry of severe acute respiratory syndrome coronavirus is mediated by the spike glycoprotein and enhanced by dendritic cell transfer through DC-SIGN. J. Virol. 78, 5642–5650.

Ying, W., Hao, Y., Zhang, Y., Peng, W., Qin, E., Cai, Y., Wei, K., Wang, J., Chang, G., Sun, W., Dai, S., Li, X., Zhu, Y., Li, J., Wu, S., Guo, L., Dai, J., Wang, J., Wan, P., Chen, T., Du, C., Li, D., Wan, J., Kuai, X., Li, W., Shi, R., Wei, H., Cao, C., Yu, M., Liu, H., Dong, F., Wang, D., Zhang, X., Qian, X., Zhu, Q., He, F., 2004. Proteomic analysis on structural proteins of severe acute respiratory syndrome coronavirus. Proteomics 4, 492–504.